Spatiotemporal Complexity of Ventricular Fibrillation Revealed by Tissue Mass Reduction in Isolated Swine Right Ventricle

Further Evidence for the Quasiperiodic Route to Chaos Hypothesis

Young-Hoon Kim, Alan Garfinkel, Takanori Ikeda, Tsu-Juey Wu, Charles A. Athill, James N. Weiss, Hrayr S. Karagueuzian, and Peng-Sheng Chen

Division of Cardiology, Department of Medicine, Cedars-Sinai Medical Center, and UCLA School of Medicine, Los Angeles, California 90048

Abstract

We have presented evidence that ventricular fibrillation is deterministic chaos arising from quasiperiodicity. The purpose of this study was to determine whether the transition from chaos (ventricular fibrillation, VF) to periodicity (ventricular tachycardia) through quasiperiodicity could be produced by the progressive reduction of tissue mass. In isolated and perfused swine right ventricular free wall, recording of single cell transmembrane potentials and simultaneous mapping (477 bipolar electrodes, 1.6 mm resolution) were performed. The tissue mass was then progressively reduced by sequential cutting. All isolated tissues fibrillated spontaneously. The critical mass to sustain VF was 19.9±4.2 g. As tissue mass was decreased, the number of wave fronts decreased, the life-span of reentrant wave fronts increased, and the cycle length, the diastolic interval, and the duration of action potential lengthened. There was a parallel decrease in the dynamical complexity of VF as measured by Kolmogorov entropy and Poincaré plots. A period of quasiperiodicity became more evident before the conversion from VF (chaos) to a more regular arrhythmia (periodicity). In conclusion, a decrease in the number of wave fronts in ventricular fibrillation by tissue mass reduction causes a transition from chaotic to periodic dynamics via the quasiperiodic route. (*J. Clin. Invest.* 1997. 100:2486–2500.) Key words: action potentials, G7.453.697.100+ • activation analysis, E5.196.39+ • tachycardia, ventricular, C14.280.67.845.940 • electrophysiology, G1.344.528+ • mathematics; H1.548+

Introduction

Ventricular fibrillation (VF)[1] is an abnormal cardiac rhythm characterized by rapid and irregular electrical activity. While this electrical activity appears to be random (1), computerized mapping studies revealed the presence of both discrete wavelets and well-formed reentrant wave fronts (2). The reentrant wave fronts were formed and terminated by specific identifiable mechanisms, indicating that activations during VF did not occur randomly (2). Compatible with these results, mathematical analyses of the electrical activations acquired directly from the ventricles during fibrillation revealed that activations during VF are not entirely random. Rather, there is a deterministic relation between successive activations (3). We define determinism to be a condition where the occurrence of a given activation is related to the preceding activation. In contrast, a random activation sequence indicates that there is no relationship between successive activations. Our group (4) recently studied fibrillation with both computer simulation and analyses of activations recorded during in vivo and in vitro atrial and VF, and found evidence for determinism during fibrillation. Furthermore, we identified a specific transition mechanism from periodicity (tachycardia-flutter) to chaos (fibrillation) in cardiac tissue: the quasiperiodic route to chaos. Quasiperiodicity, by definition, occurs when one oscillatory process is modulated by another oscillatory process with an independent frequency, resulting in aperiodic activity. As first suggested by Ruelle and Takens (5), if the system is further modulated by a third oscillatory process, it destabilizes and becomes chaotic. This scenario is the quasiperiodic route to chaos. Our discovery of a quasiperiodic route to chaos in VF strongly supports the hypothesis that cardiac fibrillation is a form of deterministic chaos.

However, the specific physiological mechanisms responsible for the generation and maintenance of the chaos in ventricular tissues remain unclear. The experiments of Garrey (6) showed that the cardiac mass is important in maintaining fibrillation. When pieces were cut away from a fibrillating ventricle, the remaining portion of the ventricle continued to fibrillate until 3/4 of the mass had been removed at which points fibrillation ceased, suggesting that a critical mass was needed to sustain VF (6). Fibrillation was later studied by Moe et al. (7) using a computer model. In that study, fibrillation, characterized by multiple wavelets and reentrant circuits, was inducible if the product (fibrillation number) of the following parameters reached a critical value: characteristic length (L), inverse of conduction velocity (T), and the inverse of a constant that determines the refractory period (K^{-2}). This fibrillation number hypothesis suggests that the physiological complexity of the cardiac fibrillation is determined in part by the characteristic length, or tissue mass. A corollary to this hypothesis is that tissue mass reduction may result in progressively less complex electrophysiological behavior, and that there exists a critical mass below which the highly complex activation patterns (fibrillation) becomes periodic (tachycardia) or quiescent (termination). The electrophysiological counterpart to Moe et al.'s

Address correspondence to Peng-Sheng Chen, M.D., Cardiology Division, Cedars-Sinai Medical Center, Rm 5342, 8700 Beverly Blvd., Los Angeles, CA 90048. Phone: 310-855-4851; FAX: 310-289-0780; E-mail: chenp@csmc.edu

Received for publication 24 January 1997 and accepted in revised form 26 September 1997.

1. Abbreviations used in this paper: APD, action potential duration; KE, Kolmogorov entropy; TMP, transmembrane potential; VF, ventricular fibrillation; VT, ventricular tachycardia.

J. Clin. Invest.

0021-9738/97/11/2486/15 $2.00
Volume 100, Number 10, November 1997, 2486–2500
http://www.jci.org

equation is the multiple wavelets and organized reentrant wave fronts that are present in VF (2). The close coupling and interaction among these electrophysiological oscillators are important in maintaining chaotic fibrillation (4). Termination of VF by a progressive reduction in the number of wave fronts should therefore be characterized by an orderly conversion of chaos to periodicity, with the quasiperiodic interaction of wave fronts becoming more evident in the transitional stage. To study VF and chaos, we performed multichannel extracellular computerized mapping and single cell transmembrane potential (TMP) recordings at the same time. Since previous experimental studies of VF and chaos (1–4, 8) used only extracellular recording techniques that register the patterns of activation, the information on cellular repolarization characteristics and their relationship to the dynamics of VF are not studied. To fill this gap of knowledge, we performed mathematical analyses of TMP to determine the dynamics of cellular activation and repolarization properties during VF at baseline and after tissue mass reduction. The results of these analyses were used to test the hypothesis that a decrease in the number of wave fronts in VF by tissue mass reduction can cause a transition from chaos to periodicity via the quasiperiodic route.

Methods

Tissue preparation

Farm pigs (27–48 kg) of either sex were used in the study. Each was premedicated with an intramuscular injection of ketamine (20 mg/kg), acepromazine (0.5 mg/kg), and atropine (0.05 mg/kg). The pigs were then anesthetized with 20 mg/kg of intravenous thiopental sodium, intubated, and ventilated with a Harvard respirator. The chest was opened via a median sternotomy. The heart was quickly removed and placed in 37°C Tyrode's solution gassed with 95% O_2 and 5% CO_2. The composition of the solution was as follows (mM): NaCl, 125.0; KCl, 4.5; $MgCl_2$, 0.5; $CaCl_2$, 0.54; NaH_2PO_4, 1.2; $NaHCO_3$, 24.0; and glucose, 5.5 (9).

The right coronary artery was cannulated with a 6-French polyethylene catheter and secured in place with a purse-string using 3-0 silk suture. The tissue was perfused with Tyrode's solution (37± 0.5°C, pH 7.35) equilibrated with 95% O_2 and 5% CO_2 at a flow rate of 30 ml/min. The atria, the left ventricle, and the ventricular septum were removed with scissors. The major branches of the coronary arteries transected by the dissection were ligated to force the perfusate to flow through the remaining cardiac tissue, which was composed primarily of the right ventricular free wall. The mass of the tissue measured 4–5.5 × 6–9 cm, with 5–7 mm thickness. The tissue was placed with the epicardial side down in a tissue bath, which was continuously superfused with oxygenated Tyrode's solution. Thereafter the tissue was both perfused and superfused.

Computerized mapping studies

At the bottom of the tissue bath was a built-in electrode array containing 509 bipolar recording electrodes in 21 columns and 25 rows (Fig. 1). The tissue bath and the electrode location were the same as that reported in a previous study (9). The recording plaque electrode array was constructed with stainless steel wires with a diameter of 0.4 mm. The wires were fully insulated except at the tips, which served as the tissue contact points. The interelectrode distance was 1.6 mm, and the interpolar distance was 0.5 mm measured from center to center. The electrodes protruded from the bottom of the tissue chamber by ~3 mm. This 3 mm clearance allowed the oxygenated Tyrode's solution to come into direct contact with the epicardial surface to maintain its viability. Because of technical difficulties, electrodes 1–32 were not used for the recording. The electrodes were connected to a computerized mapping system (EMAP; Uniservices, Auckland, New Zealand) (10). The data were acquired continuously for 8 s at 1,000 samples per second with 18 bits of accuracy. The signals were filtered with a high-pass filter of 0.5 Hz.

Recording of TMP

The endocardium, which faced up, was fully immersed in the Tyrode's solution. Transmembrane potentials were recorded from a surface cell using a standard glass microelectrode filled with 3 M KCl. This microelectrode was coupled with an Ag-AgCl wire leading to amplifiers with a high input impedance and variable-capacity neutralization (Am-2 and ME-3221; Biodyne Electronics Laboratory, Los Angeles, CA) (11). The data were acquired by AXON TL-1-40 A/D acquisition hardware and Axoclamp-2A software (Axon Instruments, Inc., Foster City, CA), and were digitized at 3.13 KHz (No.s 1–3, 6) or 1 KHz (No.s 4, 5, 7, 8) with 12 bits of accuracy.

Protocol-1

Six tissues (No.s 1–6) were included in this protocol. In all tissues, spontaneous VF occurred when the right ventricular free wall was isolated from the heart, and it persisted in the tissue bath. Spatial data from several 8-s acquisitions were acquired by the computerized mapping system while the TMPs were continuously recorded for at least 40 s. Afterwards, scissors were used to cut out a 2 × 4–cm portion of the fibrillating tissue from the boundary of the tissue distal to the perfusion site, ~15.0–16.2% of the weight of the whole right ventricular free wall (Fig. 1). If the arrhythmia continued, data acquisition was repeated. Then, an additional 2 × 4 cm portion of the tissue was cut out from the fibrillating tissue and the activations were again recorded. This process continued until the VF either terminated or was converted to ventricular tachycardia (VT). The mass that last supported VF was the critical mass for spontaneous VF. If VT continued, data acquisition was performed again, followed by further cutting of the tissue until VT terminated. The mass that last supported VT was the critical mass for spontaneous VT. All data were obtained within 3 min of the cutting procedure.

After each cut, if no VT/VF was present, the inducibility of VF or VT was tested by programmed stimulation in the remaining tissue. This procedure continued until either VF or VT in the residual tissue could no longer be induced. For regular pacing, a bipolar pacing electrode was placed at the edge of the tissue to deliver baseline pacing (S_1) with 5 ms pulse width at twice the diastolic threshold current. Another electrode was placed at the center of the tissue, at least 2 cm from the S_1 site, to deliver a premature stimulus (S_2). After eight S_1 stimuli at a cycle length of 300 ms, single, double, and triple premature stimuli (S_2, S_3, and S_4) were applied at the S_2 site with the strength of twice diastolic threshold current. If neither VT nor VF could be induced by this stimulation protocol, then a single strong S_2 with the strength of 5–99 mA was delivered after 8 S_1 to scan the diastolic period to induce reentry (12). If arrhythmia was still not inducible, rapid ventricular pacing was performed. Successful induction of VF was defined by rapid and grossly irregular ventricular activity that persisted for over 15 s. Sustained VT was defined as a monomorphic VT that lasted for over 30 s. The total duration of each experiment was ~3–4 h.

Protocol-2

One tissue (No. 7) was studied with this protocol. The purpose of this protocol was to demonstrate that the changes observed in Protocol-1 did not result from the time delay related to data acquisition. In this tissue, there was no attempt to record TMP. As soon as 8 s of computerized mapping data were acquired, the cutting procedure was performed. The entire experiment from the baseline study to the elimination of all ventricular arrhythmia lasted 15 min.

Protocol-3

One tissue (No. 8) was studied with this protocol. The purpose was to demonstrate that stable VF can persist in this preparation over a prolonged period of time without tissue mass reduction. In this tissue, VF

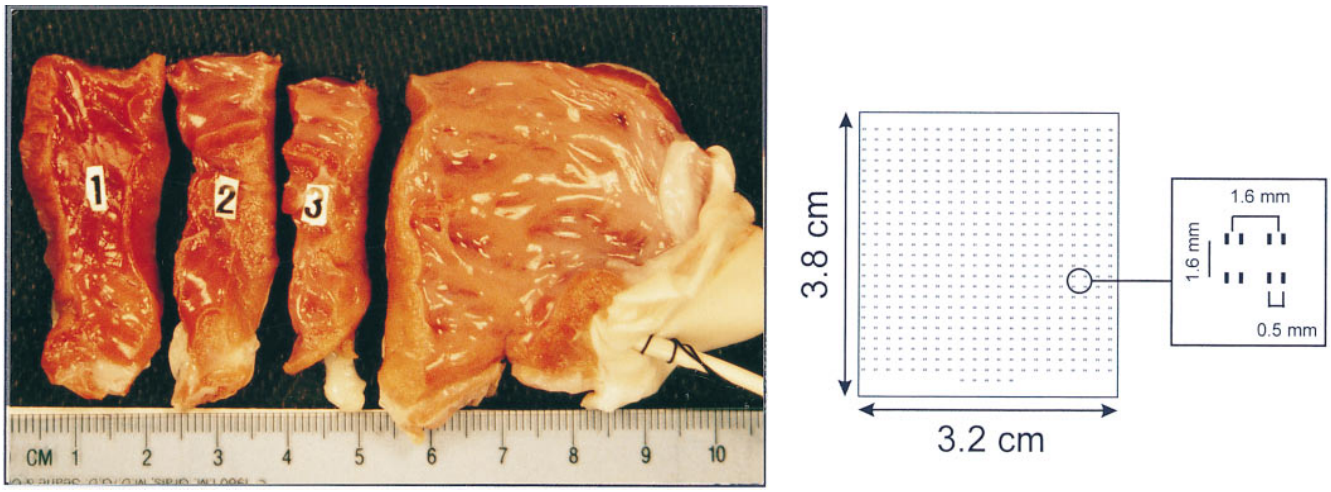

Figure 1. Example of tissue mass reduction by sequential cutting. On the left is the right ventricular free wall after cutting. No.s 1–3 indicate the sequence of cutting. The size of the remaining tissue is 3.5 × 4 cm. On the right is a schematic drawing of the plaque electrode array. There are 21 columns and 25 rows of bipolar electrodes. There are only five electrodes on the last row. Thus the total number of electrodes is 509. The smaller square is an enlarged view of four pairs of neighboring bipolar electrodes. The size of the plaque is smaller than that of remaining tissue shown on the left side of the figure. Mapping was done only in this portion of tissue throughout the experiment.

was allowed to continue undisturbed until the quality of epicardial recording deteriorated. Data were periodically acquired at 30-min intervals.

Data analysis

Transmembrane potential. Typically a 40–60-s recording of TMP before and after each cutting procedure was analyzed. The data were selected if there was a stable microelectrode recording. To measure interactivation intervals, the peaks of TMP were identified by computer. A local voltage maximum was selected as a peak of TMP whenever all points for at least "m" ms on each side fell below the maximum, which had to be at least "n" mV greater than any other local maximum in that interval. We tested multiple "m" and "n" values (Fig. 2, *A–D*, *left columns*) and found that the best criteria were "m" = 10 ms and "n" = 10 mV (Fig. 2 *C, left column*). If double potentials both satisfied these criteria, both upstrokes were counted. To further test whether or not the selection of activations by this method is appropriate, we also applied a custom-written program in which the selection of the activation is based on the criterion of $(dV/dt)_{max}$. Multiple cut-off values of $(dV/dt)_{max}$ (Fig. 2, *A–D*, *right columns*) were tested. The results showed that the criterion of $(dV/dt)_{max}$ = 5 V/s is the most appropriate (Fig. 2 *C, right column*). We analyzed the data using both the peak-picking method (criteria "m" = 10 ms and "n" = 10 mV) and the $(dV/dt)_{max}$ method (criterion = 5 V/s) (Fig. 2 *C*), and found that the results are comparable. To be consistent with our previous study (13), we report only the interactivation intervals selected with peak-picking method. The interactivation interval is defined by the time difference between adjacent peaks. Poincaré plots were constructed by plotting each successive interactivation interval against its previous value. Fourier spectra of interactivation intervals were calculated to confirm quasiperiodicity (14). Fourier-based spectral analysis was done on the same interval data set used for the Poincaré plot. In addition to peaks of TMP and the interactivation interval, other action potential variables measured were as follows: *a*) action potential amplitude; *b*) action potential duration measured at 50 and 90% repolarization action potential duration (APD_{50} and APD_{90}, respectively); *c*) maximum upstroke rate of depolarization ($[dV/dt]_{max}$); and *d*) time interval between the point of 90% repolarization and the maximum diastolic potential just before the upstroke of next action potential (diastolic interval). If an action potential occurred before 90% repolarization of the previous one, its diastolic interval was considered to be zero.

Computerized mapping of the epicardium. Analyses of data acquired by the computerized mapping system were performed according to methods published previously (2). Briefly, activations were selected as the time of the fastest slope (dV/dt) of each electrogram. The first selection was performed by the computer. Afterwards, all electrograms were visually inspected to confirm accuracy. For VF cycle length analysis, the interactivation interval of all electrodes were calculated over the entire 8-s period of data. The average of these interactivation intervals was the average cycle length for that episode of VF.

A dynamic display of activation patterns was visualized on a computer screen, in which each electrode was illuminated when an activation was registered. Each dot initially turned red, then yellow, then green, then light blue, and finally dark blue for 10 ms at each color. A reentrant wave front was defined as a wave front that completed a roughly circular pathway and reentered the area of initiation. The life-span of the reentrant wave fronts was determined by calculating the number of rotations through this circular pathway. The number of wave fronts at a given instant of VF was defined as the number of activations that were excited in different areas of the mapped tissue which had different directions of propagation and cycle length, and were clearly separated from each other by recovered but nonactivated tissue (7).

Determination of depolarized tissue mass. To determine the amount of tissue depolarized during a given interval or during a given rhythm, we calculated the number of electrodes that registered an activation (red dots) during dynamic display. Red dots were counted every 10 ms throughout the 8-s data window. These numbers represented the total mass of tissue depolarized within a 10-ms interval. A plot of these numbers versus time revealed the temporal changes of the amount of tissue depolarized in the mapped area during the evolution of an arrhythmia.

Kolmogorov entropy (KE). KE, also called Kolmogorov-Sinai entropy (15–17), is a way to measure the degree of disorder in a system. In an orderly system, the activity of the system follows a certain defined path. On the other hand, if a system is in disorder, the activity does not repeat itself. Rather, new states are frequently entered. KE provides a quantitative measure of this disorderly behavior. The idea behind KE is that if we take a point in a given cell and follow its tra-

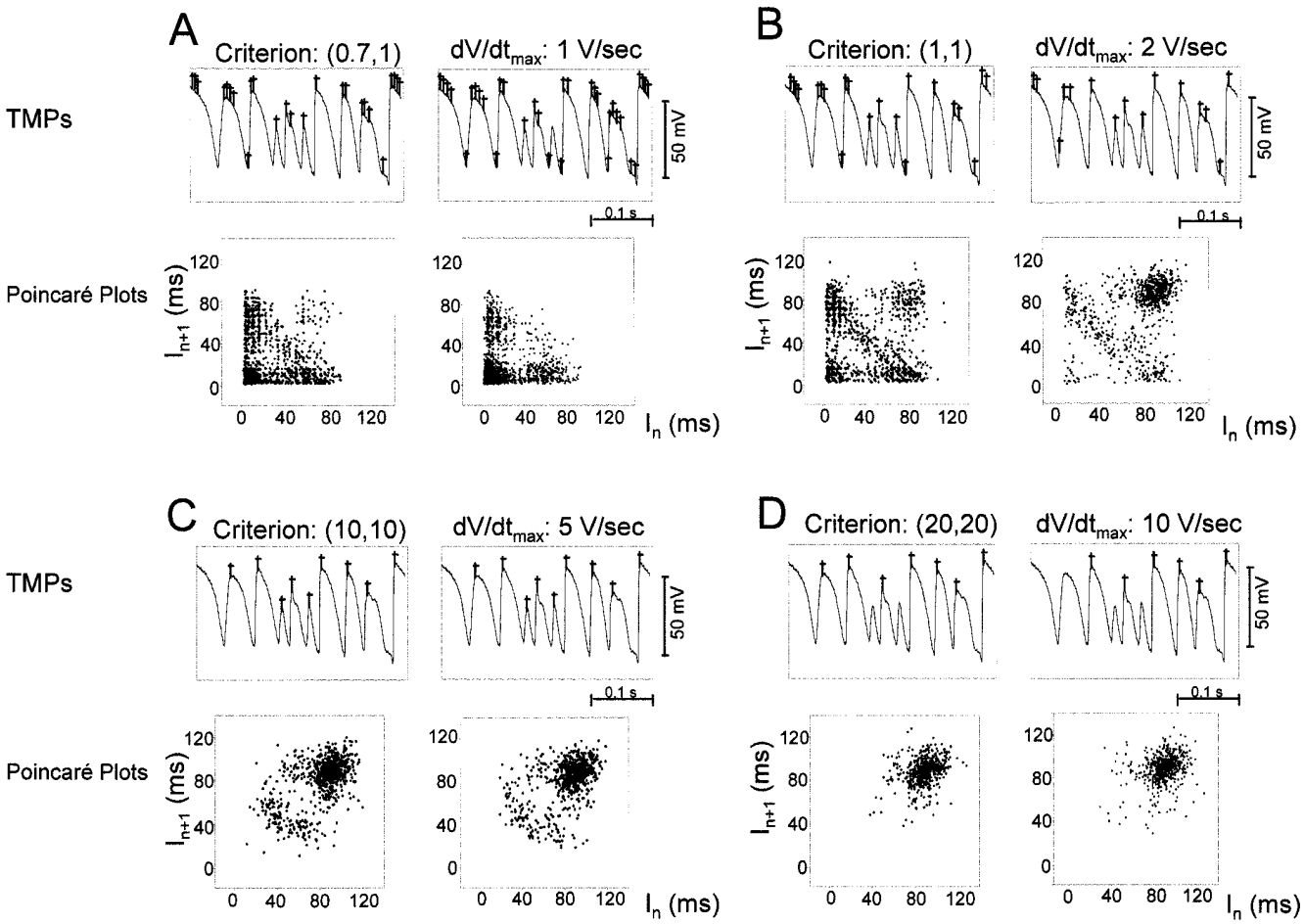

Figure 2. Comprehensive evaluation of criteria used to determine the times of activation. The upper row of each panel shows TMPs. The plus sign marks the time of activation selected by different criterion. The Poincaré plots (*lower row of each panel*) were generated based on the times of activations selected. The peaks of TMP on left columns in *A*, *B*, *C*, and *D* were selected by (m, n) criteria, whenever all points for at least m ms on each side fell below the maximum, which had to be at least n mV greater than any other local maximum. The peaks of TMP on right columns in *A*, *B*, *C*, and *D* were selected by dV/dt_{max} criteria. (*A*) (0.7, 1) criterion (*left*), 1 V/s (*right*); (*B*) (1, 1) criterion (*left*), 2 V/s (*right*); (*C*) (10, 10) criterion (*left*), 5 V/s (*right*); (*D*) (20, 20) criterion (*left*), 10 V/s (*right*). *A* shows that activations were overselected and thus divided one action potential into three or five intervals. As a result, most points were distributed in the range of 0–80 ms of interactivation intervals in the Poincaré plots. (*B*) The main frequency of activations appeared to be present in the range of 90–100 ms, because of diminished overselection of activations. However, some activations were selected inappropriately and were distributed in the area of short frequency of the Poincaré plots. (*C*) The most appropriate selection of activations and ring-like structure on the Poincaré plots; (*D*) omission of real activations, which resulted in the disappearance of a ring-like structure on the Poincaré plots.

jectory forward, the trajectory will invade new cells. The rate of invasion of new cells will be proportional to exp (Kt); K is the KE.

In this study, we calculated the KE for each data set from a 10-s sample of the TMP recordings. First, an appropriate embedding dimension was chosen using the method of false nearest neighbors (18). The typical embedding dimension was five. A delay-coordinate embedding was then created in the appropriate dimension, and the resulting state-space was coarse-grained, dividing each dimension into six bins (thus, there were typically $6^5 = 7{,}800$ cells). Suppose we start with M points in a given cell. n time points later, there will be M_r of these points in cell r. Define the probability p_r of a point being in cell r as M_r/M. The Shannon entropy at the n^{th} time point is defined as

$$S_n = -\sum_r p_r \log_2 (p_r).$$

This is a quantity that is minimized when the system visits few cells, and maximized when all cells are equally visited. Entropy is, therefore, a measure of our uncertainty of the state of a system. A chaotic system is always invading new cells, constantly creating entropy. (At least initially; for a given coarse-grain, after a longer time, a chaotic system will have settled onto an attractor, and so will not continue to occupy new cells.) The KE is defined as the average time rate of change of entropy as the system evolves. So if

$$K_n = \frac{1}{\tau}(S_{n+1} - S_n)$$

is the change of entropy at the n^{th} time step, where τ is the time between data points, then

$$K = \lim_{N \to \infty} \frac{1}{N\tau} \sum_{n=0}^{N-1} (S_{n+1} - S_n).$$

This definition is dependent on choice of bin size (side length L) and data time step τ. Theoretically, this should be removed by taking the double limit of the above quantity K, as $L \to 0$ and then as $\tau \to 0$.

In practice, we chose sufficiently small values of the two to give stable calculations. The theoretical definition of KE, for infinitely long records with an infinitely short time between data points, is defined as a triple limit: the limit of the rate of occupation of new boxes as *a*) the record length goes to infinity, as *b*) the box size goes to zero, and as *c*) the time step between data points goes to zero. In the real world, of course, none of these are possible, and so we must make approximations. We have attempted to demonstrate that our calculations of KE converge with respect to these limitations of real world data. *a*) Record length: We calculated KE for record lengths that were 2 and 3 times the length originally used. This was usually only possible in the baseline condition, as the lower frequency of activations in the later parts of each experiment meant that we had to use almost all of the record in our original calculations. For the six baseline conditions, the KE for 2 and 3 times record lengths did not vary by more than 10% of the original estimate. Since this is much less than the difference between baseline and final cut, we concluded that the effect of record length converged for the values we used. *b*) Box size: We used the smallest box size that was feasible for our data. Halving the box side length makes for 4 times the number of boxes. If the same record length were used with four times the number of boxes, the calculation would be biased downward (since most boxes would have occupancy 1 or 0, for both of which $p \log p = 0$). Since we did not have four times record length in the late cuts, we could not make the box size smaller. *c*) Time step: We used the smallest time step available in the original data, which was 1 ms in some records and 0.32 ms in others. For the high-frequency sampled data, we considered the effect of considering only a 1-ms time step, and then refined it to 0.5 ms. In each case, the results were within sampling error.

Statistical analysis. All data were presented with mean±SD and were compared by use of Student's *t* tests when appropriate. ANOVA with Newman-Keuls test was used when multiple comparisons were performed (19). A P value ≤ 0.05 was considered significant.

Results

Critical mass for ventricular fibrillation or ventricular tachycardia. Fig. 3 shows the weight of the critical mass necessary for sustaining induced VF or VT in each experiment. No.s 1–6 were performed using protocol-1 and No. 7 was performed using protocol-2. The transverse line in each bar indicates the weight at which VF (*black*) or VT (*gray*) could no longer be induced by electrical stimulation. Four pigs (No.s 3, 4, 6, and 7) showed VT as a transitional rhythm before the totally noninducible state (*white*) was reached. In three pigs (No.s 1, 2, and 5), the transition from spontaneous VF to the noninducible state after progressive tissue mass reduction did not include an intermediate VT state.

In each tissue, a critical mass existed which was necessary to sustain VF. The average weight of the critical mass for spontaneous VF was 24.0±3.4 g (74.1±16.7% of weight of right ventricular free wall, 16.1±2.7% of total weight of heart) and that for inducible VF was 19.9±4.2 g (50.0±16.7% of right ventricular free wall, 13.1±3.6% of total weight of heart), which was smaller than that of spontaneous VF ($P < 0.05$). The average weight of the critical mass for inducible VT was 13.9±3.6 g, which is equivalent to 36.1±4.8% of right ventricular free wall or 9.6±2.7% of total weight of heart. This weight is significantly smaller than the critical mass for spontaneous VF ($P < 0.05$), but was not significantly different from the critical mass for inducible VF.

The transition from higher to lower dimensional patterns. Under baseline conditions (Fig. 4), TMP records exhibited highly variable amplitude and interactivation intervals (*A*, *E*, and *I*). The series of interactivation intervals showed an irregular pattern characteristic of VF (*B*, *F*, and *J*). The Poincaré plots (*C*, *G*, and *K*), in which each successive value of interactivation interval was plotted against its next value, had either a formless cloud-like appearance (*C*) or a signet ring-like appearance (*G* and *K*). By spatial statistics (4), statistically significant holes can be defined if there are significantly fewer data points at short distances from a point in the center than at long distances. Using this criterion, No. 1 tissue after the second cut, No. 5 tissue at baseline, after the first and second cut, and No. 8 tissue at all times showed statistically significant holes, corresponding to their ring-like appearance in the Poincaré plots. To determine whether Fourier spectra of interactivation intervals revealed significant power in low frequency (*D*, *H*, and *L*), spectra were binned into 20 equal width bins, and the statistical significance of the count in the lowest frequency bin was assessed by comparing it to the result of similarly analyzing 100 random permutations of the original interval series (Fig. 5). In all cases of VF at baseline, there was more low-frequency power (in the lowest bin) in the actual case than for 95 out of 100 of the shuffled series. Therefore, there was statistically significant low-frequency modulation in VF, with $P \leq 0.05$. The low frequency modulation corresponded to a period from 8 to 40 interactivation intervals. Given a mean interactivation interval of 95 ms at the baseline, this means that roughly every 0.8–3 s a secondary modulation of interactivation intervals occurred.

In Fig. 6, *A*, *D*, *G*, and *J* show TMP recorded at baseline and after each cut. *B*, *E*, *H*, and *K* show the Poincaré plot of interactivation intervals in successive cuts in a single experiment. The progression from a cloud-like pattern (highest in complexity) to a ring-like pattern (medium complexity) to a point-like pattern (lowest complexity) is evident over the three cuts. In other cases, however, a cloud-like pattern persisted for all cuts

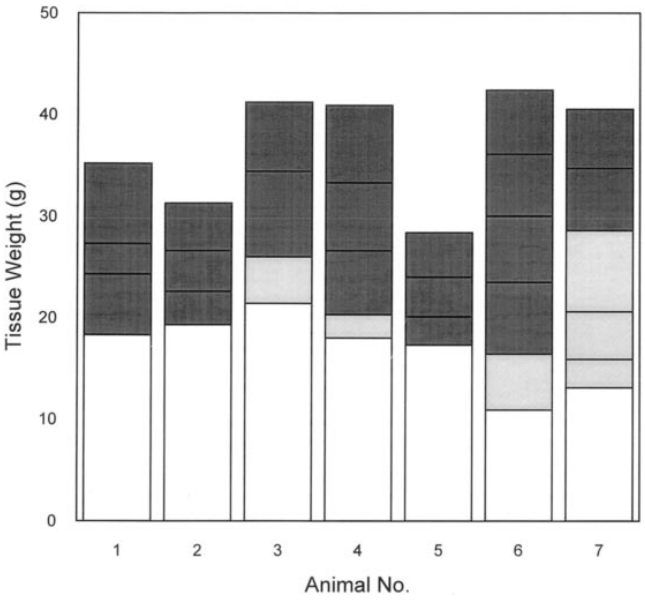

Figure 3. Critical mass for sustaining spontaneous or induced ventricular fibrillation (*VF*, *black*) or ventricular tachycardia (*VT*, *gray*) in each experiment. Transverse line in each bar indicates the weight after each cutting before the arrhythmia became noninducible (*white*). Pigs 1–6 were done with protocol-1; No. 7 was studied with protocol-2.

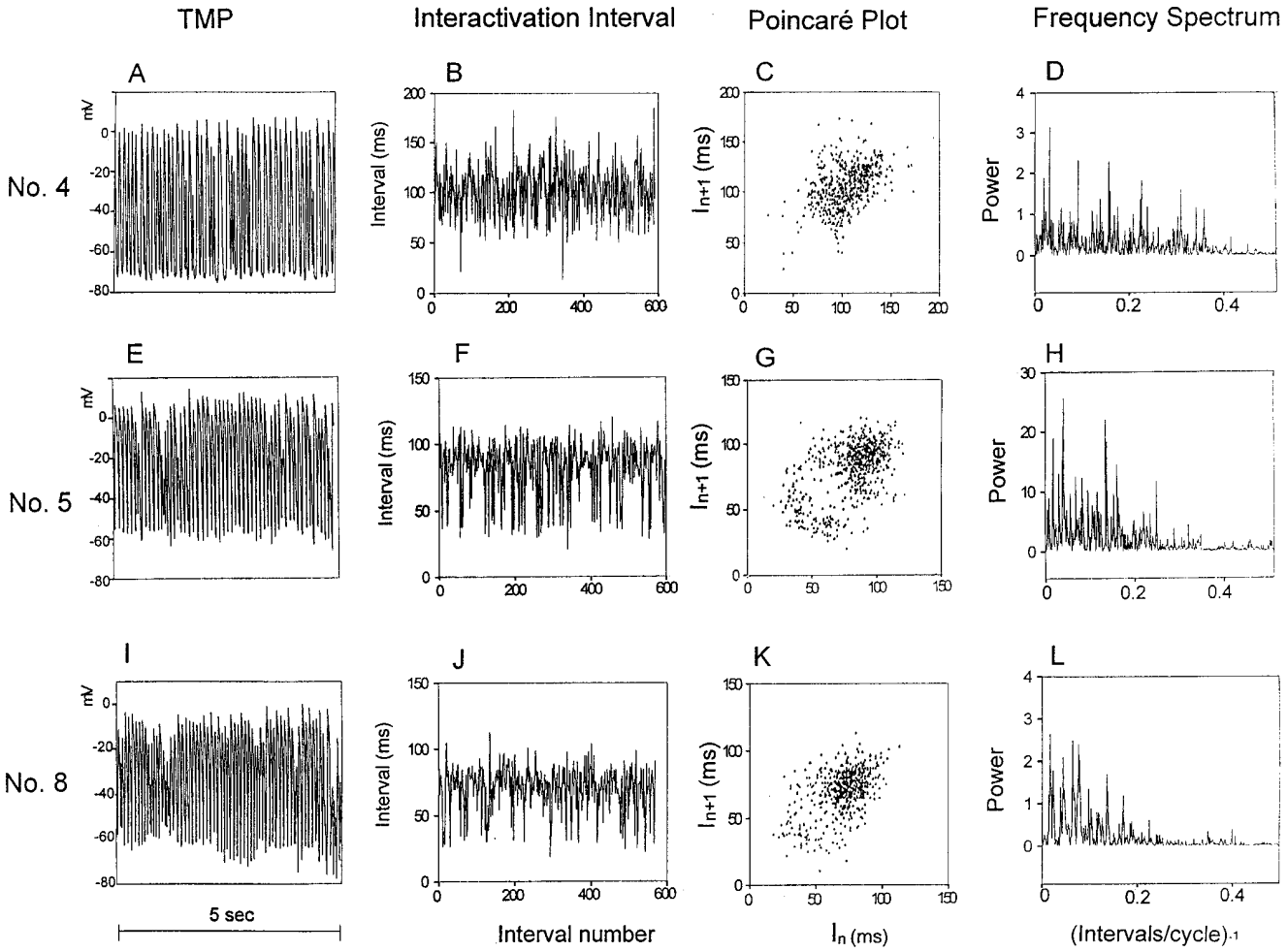

Figure 4. Analysis of TMP recordings at baseline. The data were from hearts No. 4 (*A–D*), 5 (*E–H*), and 8 (*I–L*). *A*, *E*, and *I* show TMP during 5 s of ventricular fibrillation at baseline. *B*, *F*, and *J* show time series of interactivation intervals over a 60-s period. *C*, *G*, and *K* are Poincaré plots of I_{n+1} against I_n, where I indicates interactivation interval. *D*, *H*, and *L* show Fourier spectra of interactivation intervals. The power on the ordinate has arbitrary units. The abscissa is in (interactivation intervals/cycle)$^{-1}$. For example, period-2 (alternans) has two interactivation intervals/cycle, i.e., the (intervals/cycle)$^{-1}$ of 0.5.

(No. 2), and sometimes ring-like pattern was seen even at baseline (No. 5). However, with all of the 18 cuts in the six hearts, we never observed an increase in the complexity of the Poincaré plot in any case, and in six a decrease was observed (Table I).

The presence of quasiperiodic modulation was also confirmed by calculating frequency spectra from the interval series for each experiment (Fig. 6, *C*, *F*, and *I*). As tissue mass was reduced, decreasing complexity in the time series of TMP was manifested by less frequent large-scale modulations of amplitude (Fig. 6, *A*, *D*, *G*, and *J*). The decrease in dynamical complexity was also quantified by calculating Kolmogorov entropies for each stage of each experiment. The results are shown in Fig. 7 *A*: KE decreased in all but one of the 18 cuts, and was significantly lower after the second and third cut, compared with baseline or after the first cut. For each animal, we counted the number of activations per 10 s for each cut. The number decreased from ~ 154 at baseline to 133 after the first cut, 100 after the second cut, and 62 after the third cut. To determine whether or not fewer activations in later cuts affected the entropy calculation, we reanalyzed these data by creating proportionately longer records for the later cuts and subjecting the resulting time series to the same KE calculation. The mean value of these data (Fig. 7 *B*) showed results similar to those of Fig. 7 *A*, but significantly lower only after the third cut.

Table I. Changing Patterns of Poincaré Plots

Animal no.	Baseline	First cut	Second cut	Third cut
1	Cloud	Cloud	Ring*	Point*
2	Cloud	Cloud	Cloud	Cloud
3	Cloud	Cloud	Cloud	Point*
4	Cloud	Cloud	Cloud	Point*
5	Ring	Ring	Ring	Point*
6	Cloud	Cloud	Cloud	Point*
	Baseline	1 h	2 h	4 h
8	Ring	Ring	Ring	Ring

*Decrease in complexity.

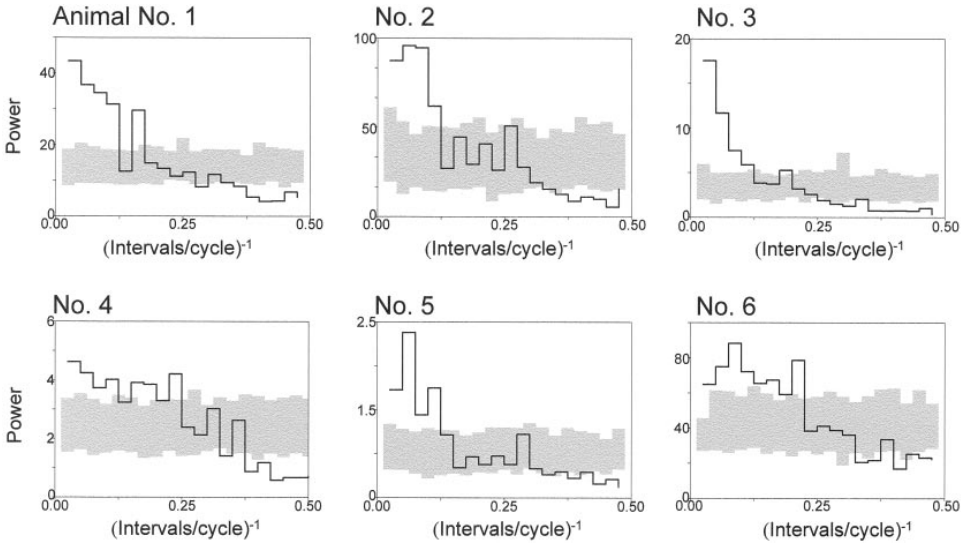

Figure 5. Fourier spectra of interactivation intervals in all tissues. The heavy black lines represent the actual data, while the shaded gray regions are the 95% confidence intervals for the same data in randomized order. Thus any part of the black line outside of the gray area is significant with $P < 0.05$. Note that in each animal, there was significant low frequency modulation of the interactivation intervals.

These changes were not due to progressive tissue deterioration over time because in the control pig (No. 8), the patterns of TMPs (Fig. 8, *A*, *D*, and *G*) and the morphology of the Poincaré plot (*B*, *E*, and *H*) were not different over a 4-h period. Fourier spectra (*C*, *F*, and *I*) were also not significantly different in the behavior of low frequency modulation within this period.

Changes in the characteristics of transmembrane potentials. The decreasing dynamical complexity with tissue mass reduction was also accompanied by changes in the TMP characteristics. In the seven examples of VF, the mean interactivation interval increased from 92.7±17.1 ms, to 99.8±18.4 ms (P = NS versus baseline), to 128.0±21.4 ms, and to 137.5±15.6 ms, after the first, second, and third cuts, respectively ($P < 0.01$).

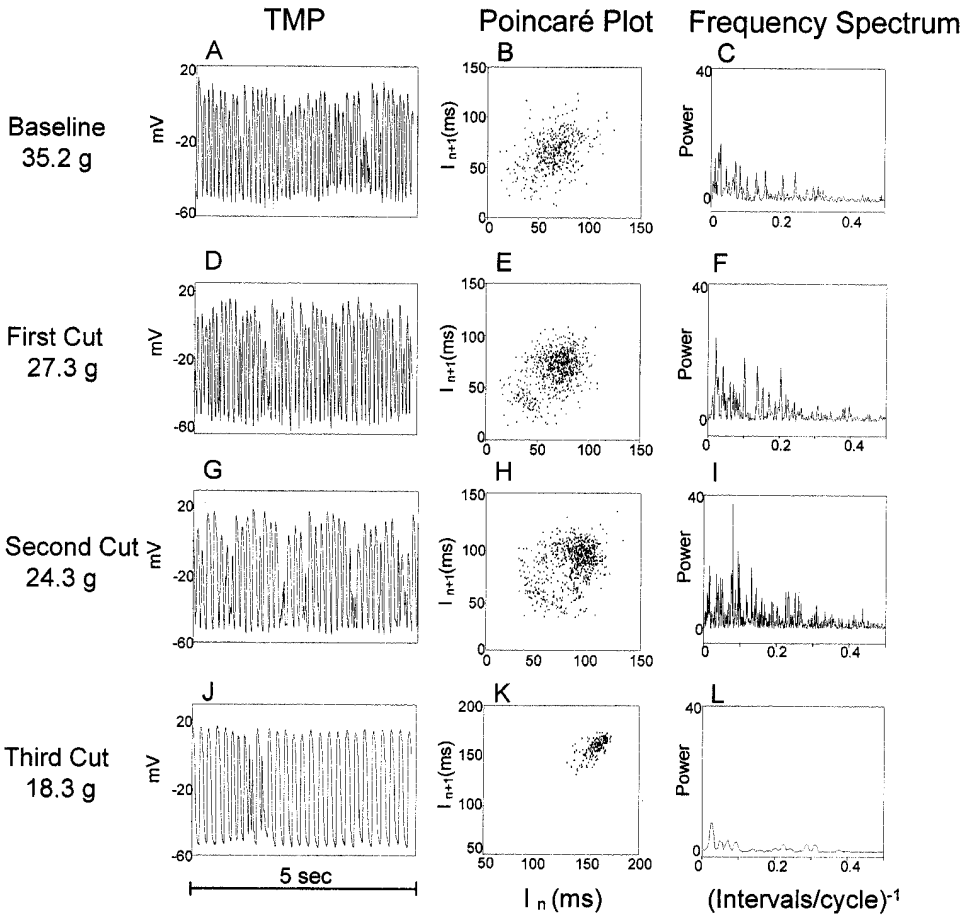

Figure 6. Transition from VF to VT state with reduction of tissue mass. TMP (*A*, *D*, G, and *J*), Poincaré plots of I_{n+1} against I_n (*B*, *E*, *H*, and *K*), and Fourier spectra of interactivation intervals (*C*, *F*, *I*, and *L*) are shown at baseline, and after the first, second, and third cuts, respectively. At baseline (*B*), the Poincaré plot was structureless, indistinguishable from randomness or high dimensional chaos. After the first cut, the Poincaré plot (*E*) began to show ring-like structure, and Fourier spectrum (*F*) showed low frequency modulation, reflecting the underlying quasiperiodic modulation. After the second cut, the signet-ring like appearance in the Poincaré plot became even clearer (*H*), and the recording of TMPs (*G*) showed low frequency modulations in both amplitude and interval, consistent with the low frequency power in the frequency spectrum (*I*). After the third cut, TMP (*J*) showed transition from VF into VT and Poincaré plot of the VT portion (*K*) demonstrated period-1. Frequency spectrum (*L*) showed weak power at all frequencies, indicating little variation of intervals, that is, regular periodicity.

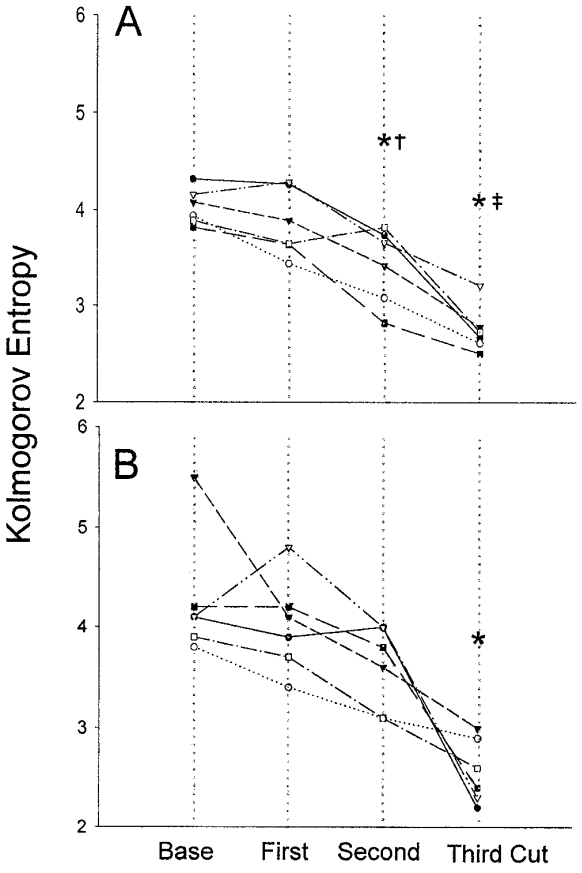

Typically, as shown in one example of TMP data in Fig. 9, mean APD_{50} and APD_{90} did not differ between baseline (54.8±34.7 ms, 78.3±38.4 ms, respectively) and after the first cut (57.7±41.2 ms, 79.8±41.2 ms, respectively, P = NS versus baseline), but were prolonged significantly after the second cut (59.8±37.7 ms, 84.8±37.4 ms, respectively, $P < 0.01$) and after the third cut (64.2±30.8 ms, 91.8±28.3 ms, respectively, $P < 0.01$). As the tissue was reduced in mass, diastolic interval increased progressively ($P < 0.01$). It was 11.8±4.5 ms (12.3±11.9% of cycle length) at baseline, 18.2±12.2 ms after the first cut, 34.2±12.4 ms after the second cut, and 38.3±18.2 ms after the third cut. The $(dV/dt)_{max}$ (18.4±6.6 V/s) and AP amplitude (56.2±16.7 mV) did not change significantly after the first cut (17.5±7.7 V/s and 56.1±19.1 mV, respectively) and second cut (21.4±6.9 V/s and 60.6±16.3 mV, respectively, P = NS). However, after the third cut, $(dV/dt)_{max}$ (30.2±7.8 V/s) and AP amplitude (72.7±28.4 mV) increased significantly ($P < 0.01$).

Changes in activation patterns. Fig. 10 shows a typical bipolar electrogram recording during stable, sustained VF. The morphology of the bipolar electrogram was highly variable, with many rapid deflections of various amplitudes, directions, and cycle lengths. However, the overall inter-activation intervals and the electrogram morphology did not change signifi-

Figure 7. Decrease in KE with tissue mass reduction. (*A*) Calculated values of KE (in bits) after each cut. (*B*) KE calculated after the data were adjusted by creating proportionately longer records for the later cuts. *$P < 0.01$ versus baseline. †$P < 0.05$, ‡$P < 0.01$ versus first cut.

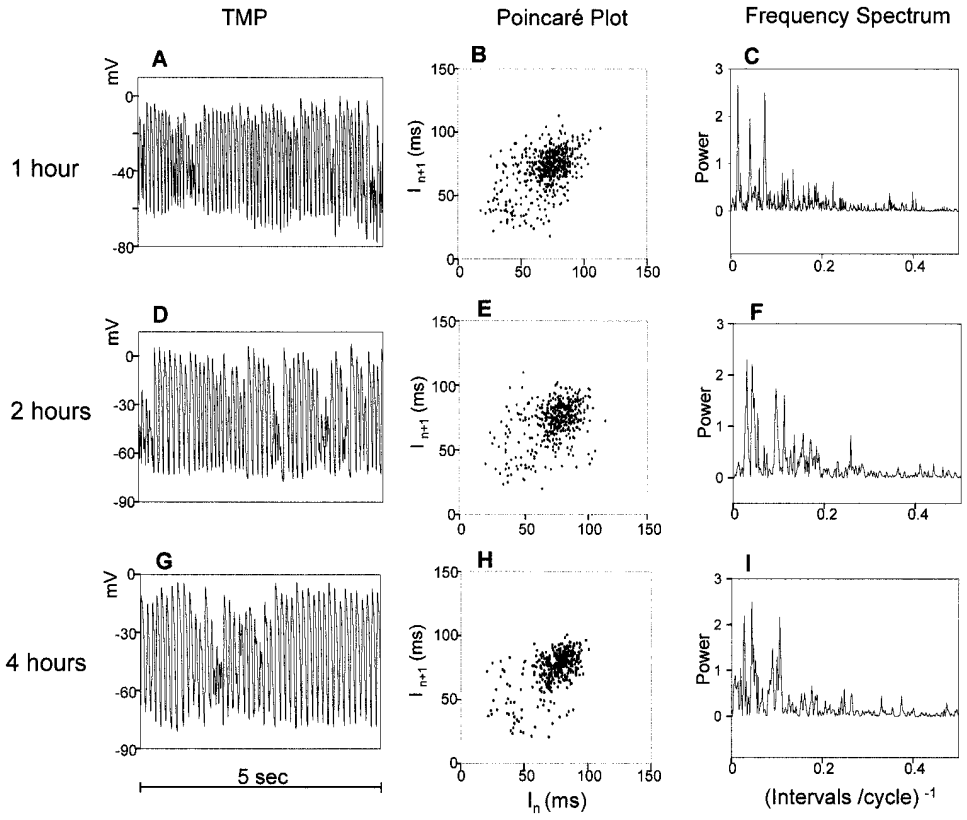

Figure 8. Control study (protocol-3). TMP (*A*, *D*, and *G*), Poincaré plots (*B*, *E*, and *H*), and Fourier spectra of interactivation intervals (*C*, *F*, and *I*) in pig No. 8 over a 4-h period. TMPs, Poincaré plots, and Fourier spectra after 1 h (*A–C*), 2 h (*D–F*), and 4 h (*G–I*) did not differ significantly.

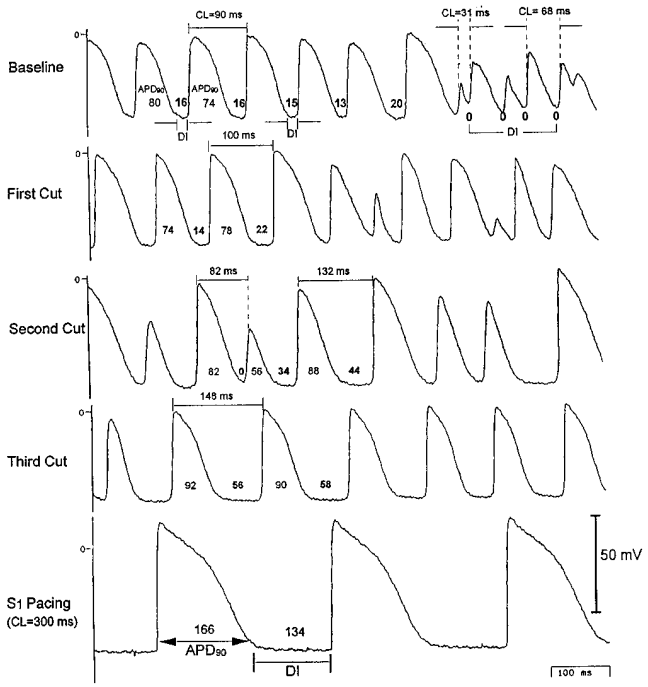

cantly over a 4-h period in pig No. 8 (protocol-3) without cutting (*A* and *C*). In contrast, interactivation intervals increased progressively after the second cut in pig No. 1 of protocol-1 (Fig. 10 *B*). In addition to lengthening of intervals, the pattern of activations became less irregular after the second cut, and became almost regular after the third cut.

Fig. 10 *D* shows that interactivation intervals increased progressively with decreasing tissue mass in all tissues of protocols-1 and -2, consistent with the TMP recordings. The mean values of these intervals were 102.6±10.9 ms during baseline, 107.6±13.9 ms after the first cut (P = NS), 138.5±16.4 ms ($P <$ 0.01) after the second cut, and 144.1±27.8 ms ($P < 0.01$) after the third cut. While the first cut had little effect on the activation patterns of VF, second or further cuts caused more promi-

Figure 9. Changes in the characteristics of transmembrane potentials with tissue mass reduction in one example (No. 4). The upper four panels demonstrate that as the tissue mass was reduced by cutting, the average cycle length (*CL*) and the diastolic intervals (*DI*) increased. The APD_{90} increased after second cut. The bottom panel shows the action potential during S_1 pacing (300 ms).

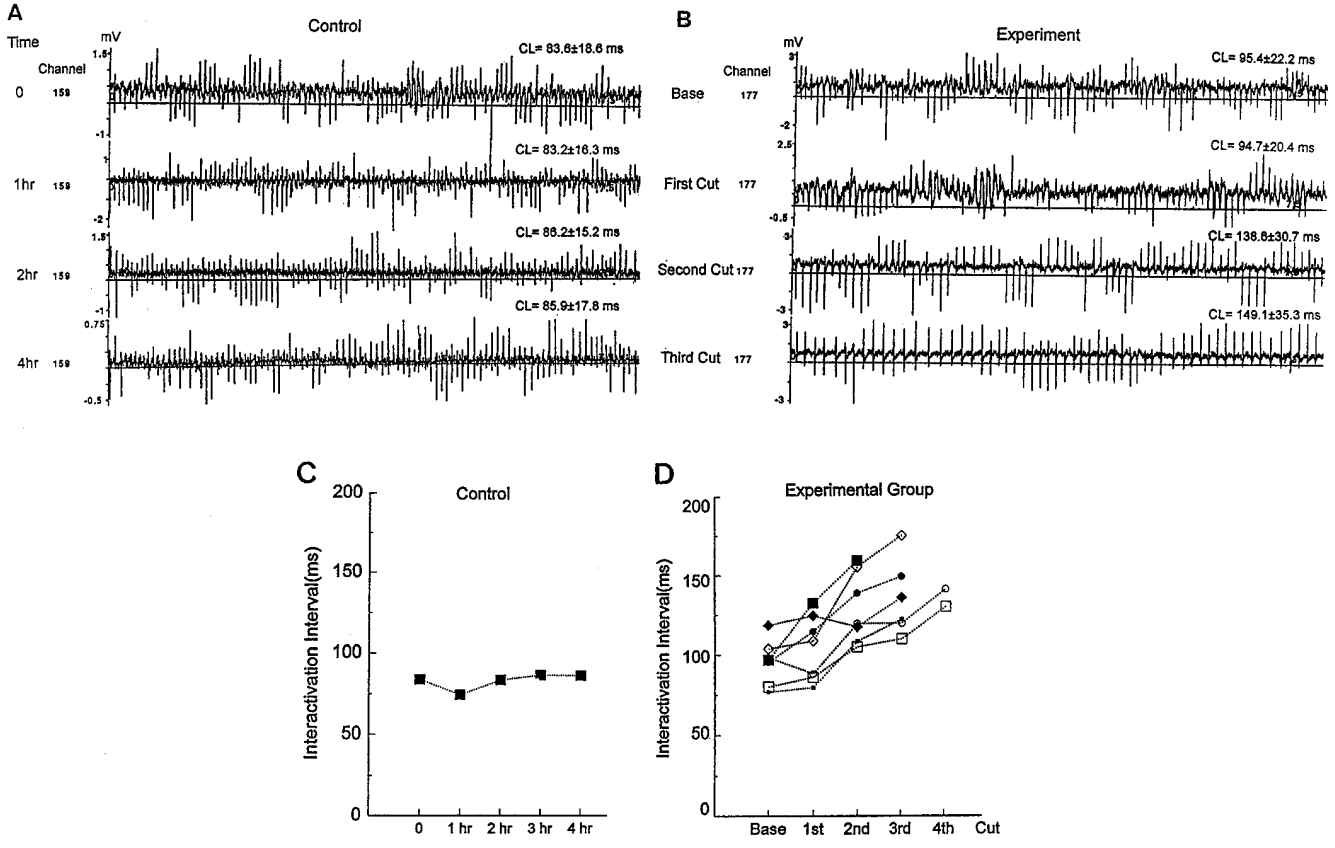

Figure 10. Activations recorded by the mapping system. (*A*) Activations during VF in pig No. 8 (protocol-3) that did not undergo tissue mass reduction. Over a 4-h period, the morphology of electrogram and the interactivation intervals did not change significantly. (*B*) Activations recorded in pig No. 1. Activations became progressively more regular and the interactivation intervals progressively prolonged as the tissue mass was reduced. *C* (No. 8) and *D* (No.s 1–7) summarize changes in the mean value of interactivation intervals. While the interactivation intervals remained unchanged in the control, they increased progressively in the experimental group as the tissue mass was reduced.

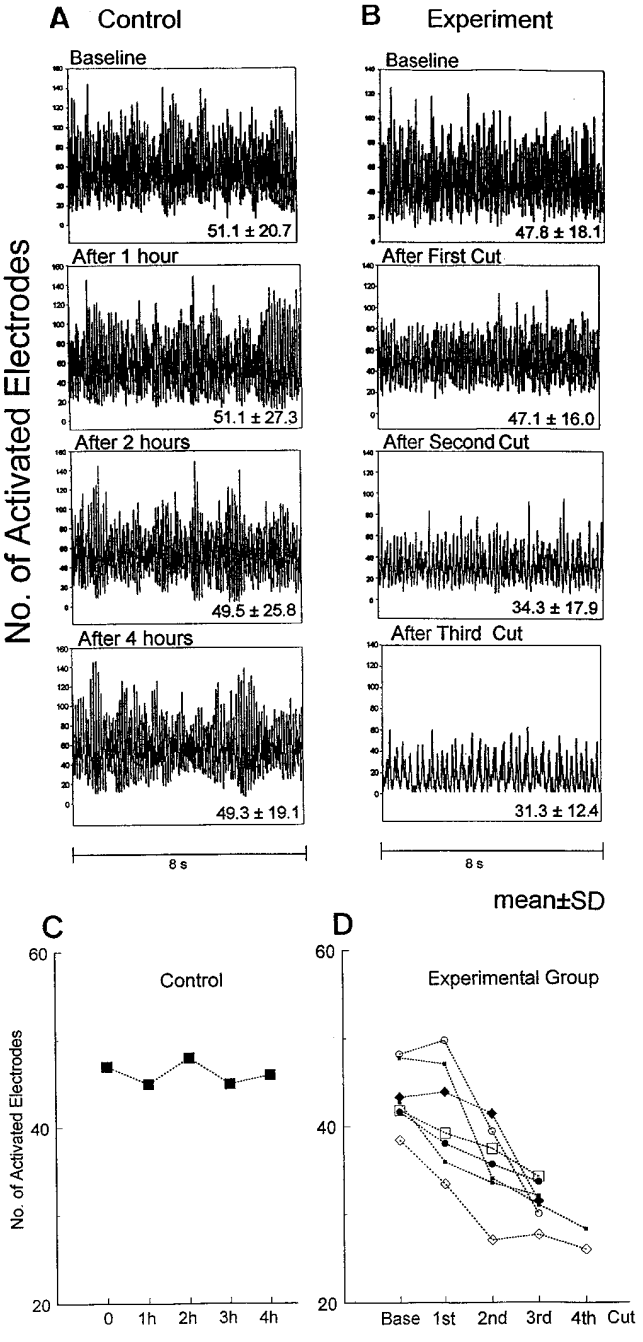

Figure 11. The amount of tissue activation in control pig No. 8 (*A*) and experimental pig No. 1 (*B*). The number of activated electrodes (ordinate) during each 10 ms is plotted against time (abscissa). (*A*) Patterns of activation and the mean number of activated electrodes (*C*) were not changed significantly over a 4-h period, during which tissue mass was not reduced. In contrast, in pig No. 1 (*B*), the number of activations had highly variable amplitude and intervals at baseline, but became progressively more periodic, with less temporal variations as the tissue mass was reduced. (*D*) Decrease in the mean number of activated electrodes after the second, third, and fourth cuts. The numbers in *A* and *B* represent the mean number of electrodes registering an activation.

nent changes, indicating that the activation intervals were strongly influenced by the size of the mass of tissue.

Changes in the amount of tissue activated. Fig. 11 illustrates the amount of tissue activated as evidenced by the number of activated electrodes (red dots in Fig. 12 *A*) during an 8 s map of VF. On the ordinate is the number of activated electrodes during each 10 ms period, and time is on the abscissa. The number of activated sites in pig No. 8 (which underwent no cuts) shown in *A* and *C* revealed no significant changes in the pattern and the average value over a 4-h period. Fig. 11 *B* shows the characteristic changes with tissue mass reduction (data from tissue No.1). The number of electrodes that registered activation, as well as the variance, decreased as the tissue mass was reduced progressively.

Fig. 11 *D* shows the decrease in the average number of electrodes that registered activations in each experiment after the second and third cuts. The amount of tissue activated at each 10 ms time interval decreased from 10.0±3.8% (47.8/477 electrodes) at baseline to 7.2±3.8% (34.3/477) after the second cut and to 6.6±2.6% (31.3/477) after the third cut ($P < 0.01$).

Number of wave fronts. All tissues in VF at baseline had multiple (mean: 3.1±0.3, maximum: 4.5±0.6) wave fronts within the mapped region. A significant number of these wave fronts had their earliest activation site within the mapped region, most likely representing epicardial breakthrough of transmural activation. Also, wave fronts arrived at the mapped region from all directions. There was no apparent preference of the earliest site of activation. The waves traveled either along or across the fiber orientations. With tissue mass reduction, the mean number of wave fronts decreased. Fig. 12 *A* shows changes in the number of wavelets that were present at selected moments in each stage in one example. Before the second cut, four multidirectional wavelets of different mass were present. After the second cut, only two wavelets were observed, and after the third cut, a single spiral wave was present. Fig. 12 *B* summarizes the results in the seven pigs. The mean number of wavelets during 8 s map of VF analyzed was higher at baseline, and decreased as the tissue became smaller after the second cut ($P < 0.01$). The maximum number of wavelets at a given instant during 8 s of VF was 4.5±0.6 at baseline, 4.0±0.7 (P = NS) after the first cut, 2.8±0.6 ($P < 0.01$) after the second cut, and 1.7±0.4 ($P < 0.01$) after the third cut. One reason for the reduced number of wave fronts is that, with each cut, less tissue was present outside of the mapped region so that fewer wave fronts were seen invading the edge of the tissue. Vanishing of existing wave fronts was also caused by fusion or collision with another wavelet and by disappearing at the border of mapped region. Fig. 13 shows an example of reentry termination when the reentrant wave front meandered and reached the boundary. Fig. 13, *A–G* show functional reentry with multiple rotations. When the wave front came close to the boundary (lower edge of the tissue), the reentry terminated (Fig. 13 *H*). An outside wave front then invaded the mapped region from the left lower edge (Fig. 13 *I*). Fig. 13 *J* shows the trajectory of the tip of the reentrant wave.

Reentrant wave fronts. Reentrant wave fronts were occasionally seen during VF (Fig. 13). Most reentrant wave fronts were initiated by perpendicular intersection of two wavelets (2). The mean life-span (No. of complete rotations) of reentrant wave fronts was 2.0±1.0 at baseline and 2.8±1.8 after the first cut (P = NS). It increased after the second cut (4.5±2.8, $P < 0.01$) and the third cut (6.8±4.0, $P < 0.01$) (Fig. 14 *A*). Thus, as the fibrillating tissue was reduced in mass, the decrease in the number of wavelets was accompanied by a significant increase in the life-span of reentrant wave fronts. This finding suggests that multiple individual wavelets that are present

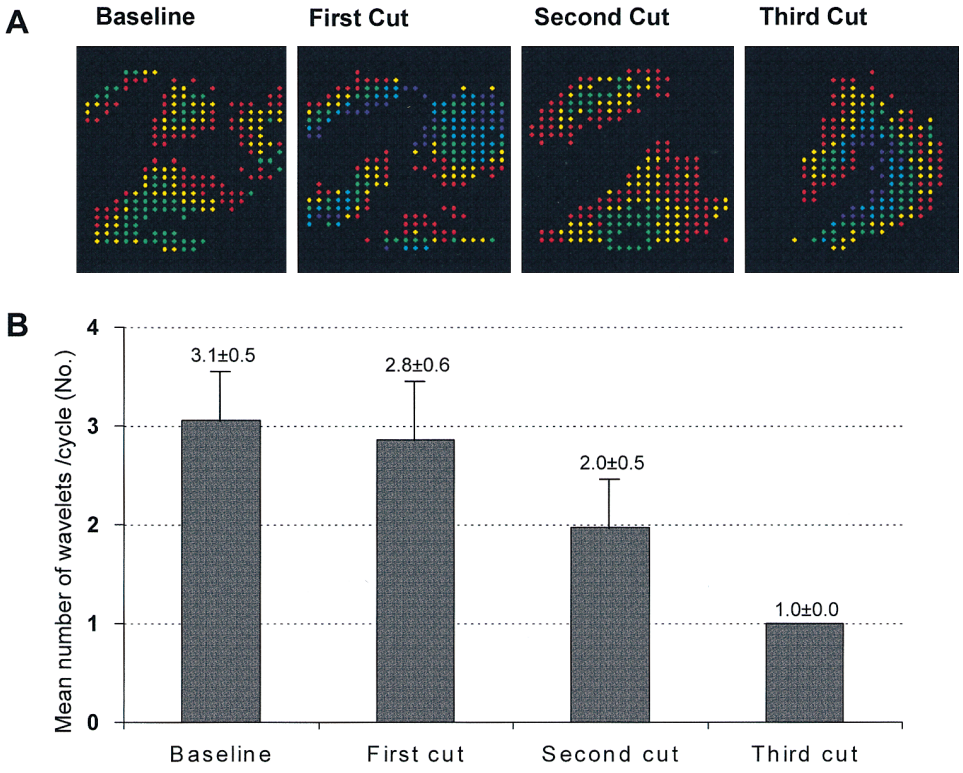

Figure 12. Changes in the number of wavelets with tissue mass reduction in pig No. 4. (*A*) The red dots represent the electrodes activated within the last 10 ms and thus indicate the leading edge of the wave front. The color then changed to yellow, green, and blue every 10 ms before returning to background black. The wavelets were considered to be different if they had different original sites of propagation and were clearly separated from other wavelets by a black (nonactivated) area at any moment. Before the third cut, multiple and multidirectional wavelets were present. After the third cut, a single reentrant wave front in which the core was located in the center of the mapped tissue appeared. (*B*) The mean number of wavelets during 8 s of VF. The number on the top of each column represents the mean±SD.

within a large mass of tissue might interfere with the reentry of a single wave front, causing premature termination. In smaller tissues, the reduction of the number of total wave fronts make this interference less likely, allowing each reentrant wave front to persist longer. The mean cycle length of reentrant wave fronts at baseline was 97.1±18.7 ms. The differences between the mean cycle length of reentrant wave fronts at baseline and after the second and third cuts were statistically significant ($P < 0.01$ for both comparisons, Fig. 14 *B*). This finding is comparable to the increase in VF cycle length measured by interactivation intervals in 477 bipolar electrograms (Fig. 10, *B* and *D*). The cycle length of reentry after each cut was not sig-

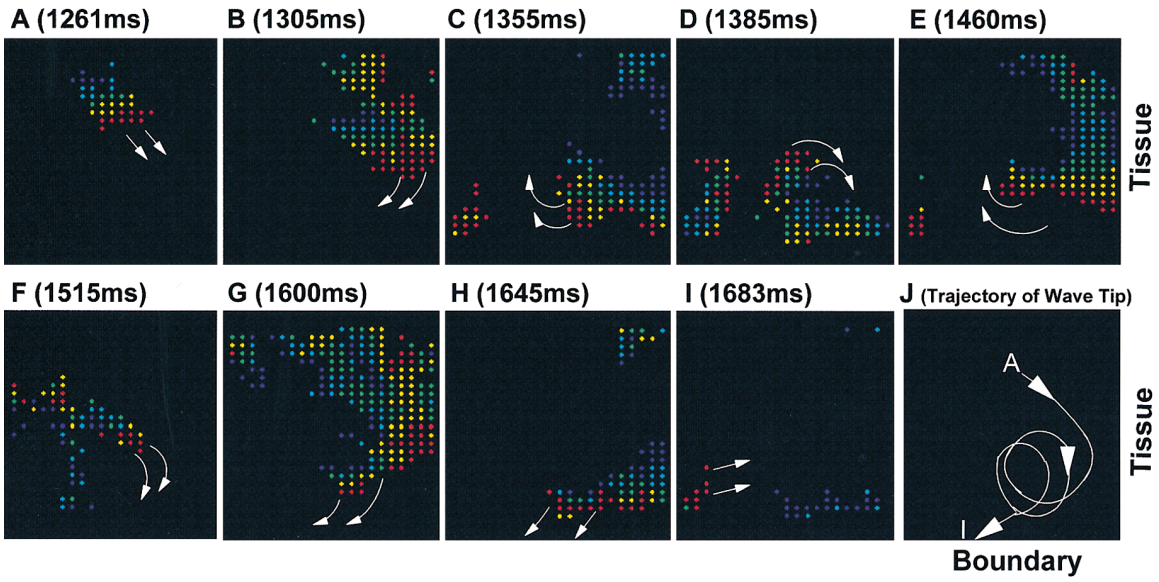

Figure 13. Termination of reentry by interaction with boundary. (*A–I*) Selected frames from the dynamic display of activation patterns during VF. With the beginning of data acquisition as time zero, the time of each frame is shown in the parentheses above each frame. (*A–F*) One reentrant wavefront rotated two cycles in a clockwise direction. It drifted from the upper to the lower center. (*G* and *H*) This reentrant wavefront drifted further toward the boundary, and finally terminated by arriving at a boundary. After termination, a new wavefront invaded the mapped region from the left lower corner (*I*). (*J*) shows the trajectory of tip motion of wavefront in *A–I*.

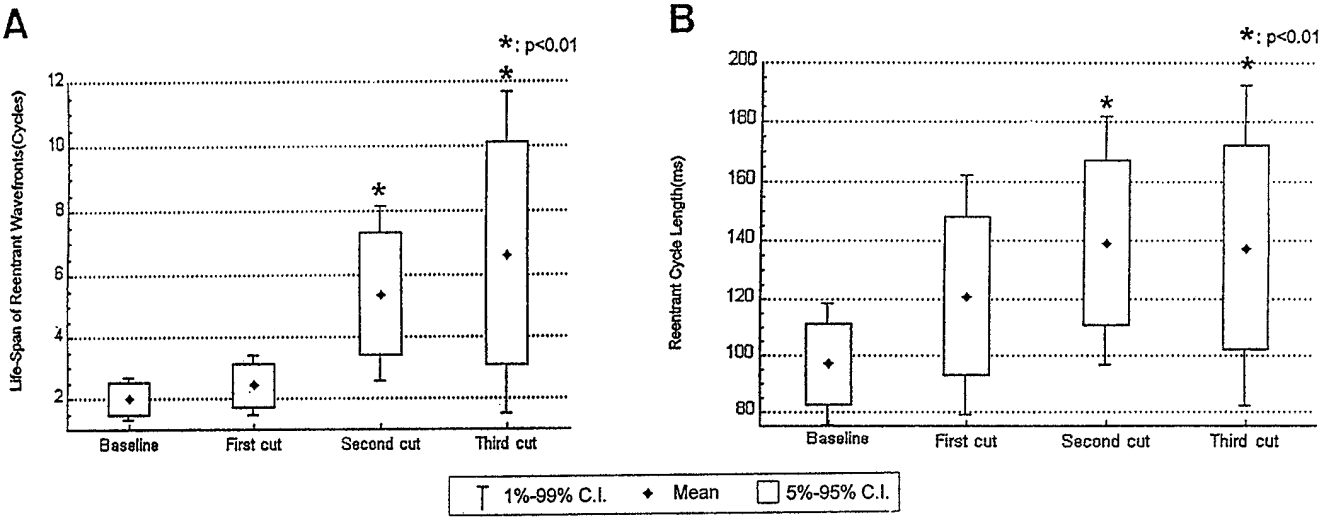

Figure 14. Life-span and cycle length of reentrant wave fronts. (*A*) Life-span of reentrant wave fronts with tissue mass reduction. After the second and third cut, the mean life-span of reentrant wave fronts significantly increased. (*B*) The cycle length of reentrant wave fronts increased as the tissue mass was decreased.

nificantly different from the cycle length of VF (after first cut, 110.7±26.3 ms; after second cut, 139.3±27.1 ms; after third cut, 137.2±21.4 ms).

Drifting of a single reentrant wave front. Fig. 15 illustrates one example of drifting of a single reentrant wave front after the third cut, resulting in VF-like activity in the extracellular recordings. Panels *A–I* are selected frames from a dynamic display of activation patterns during VF. The bottom panel shows electrograms in or near the core corresponding to the sites labeled *a* and *b* in panels *A–I*. *J* shows the trajectory of wave tip. Bipolar recordings at sites *a* and *b* showed double potentials when the core of reentrant wave front visited the recording sites. These findings demonstrate that visitation of the core of a reentrant wave front produced double potentials in bipolar electrograms and that drifting or meandering of a single reentrant wave front can give rise to fast and irregular electrograms, characteristic of fibrillation (20, 21).

Discussion

There are two major findings in this study. First, tissue mass reduction resulted in the reduction of the total number of wavelets and significantly altered TMP characteristics of VF. Second, there was a parallel decrease in the dynamical complexity before VF converted to more regular arrhythmias or terminated. These findings suggest that the wandering wavelets and reentrant wave fronts in VF contain the physiological oscillators responsible for producing complex dynamics through their interactions. By reducing tissue mass, the substrate available for these oscillators to generate spatially complex patterns diminishes. When a critical tissue mass is reached, VF either terminates or converts to a periodic rhythm characterized by a single reentrant wave front.

Decreasing complexity. Our first significant finding is that by many different measures, the complexity of the electrical activity decreases with decreasing tissue mass. This is significant because it conforms to the mathematical theory of spatiotemporal chaotic systems (22–24). Spatiotemporal chaos is distinct from purely temporal chaos because of several special properties. First, the spatial component plays an essential role in the creation and maintenance of the chaos. As opposed to a system composed of many local chaotic elements uncoupled from each other in which a local record does not show the effects of changes occurring elsewhere in the system, in true spatiotemporal chaos, a record at a single site does show the effects of distant changes. Therefore, it is significant that we see in our records exactly this local effect of distant change. For example, the KE is calculated from the voltage record made at a single site, yet it clearly changed when distant sites in the system were removed by tissue mass reduction.

A second property of spatiotemporal chaos is that the complexity of the behavior scales up (or down) with the physical mass of the system (22, 23), since the greater the mass, the more degrees of freedom a spatiotemporal system has. We observed that the number of wavelets decreased with tissue mass reduction. These wavelets are natural candidates for the degrees of freedom.

Quasiperiodic transition to chaos. Mathematicians predicted in 1971 that systems consisting of three or more independent coupled oscillations would be unstable, and degenerate into chaos (5). Since their mathematical demonstration, experimentalists have shown that such quasiperiodic transitions to chaos do occur in a number of systems, such as the transition to turbulence in fluids (26). Recently, our group presented evidence for quasiperiodic transitions to chaos in cardiac fibrillation (4). We suggested that several kinds of fibrillation showed signs of having arisen from quasiperiodic transitions. Among the most important of these signs were the presence of a ring-like structure in Poincaré plots and the presence of low-frequency modulation of intervals (the quasiperiodic oscillations) persisting into the chaotic regime, as revealed by Fourier analysis of the interval sequences. Both these signs were found in this study. In our previous study (4), we also observed several transitions from periodicity to quasiperiodicity to chaos in records of extracellular electrograms during the development of VF. However, this sequence occurred spontaneously for unclear reasons, and was not produced by any identifiable change in an

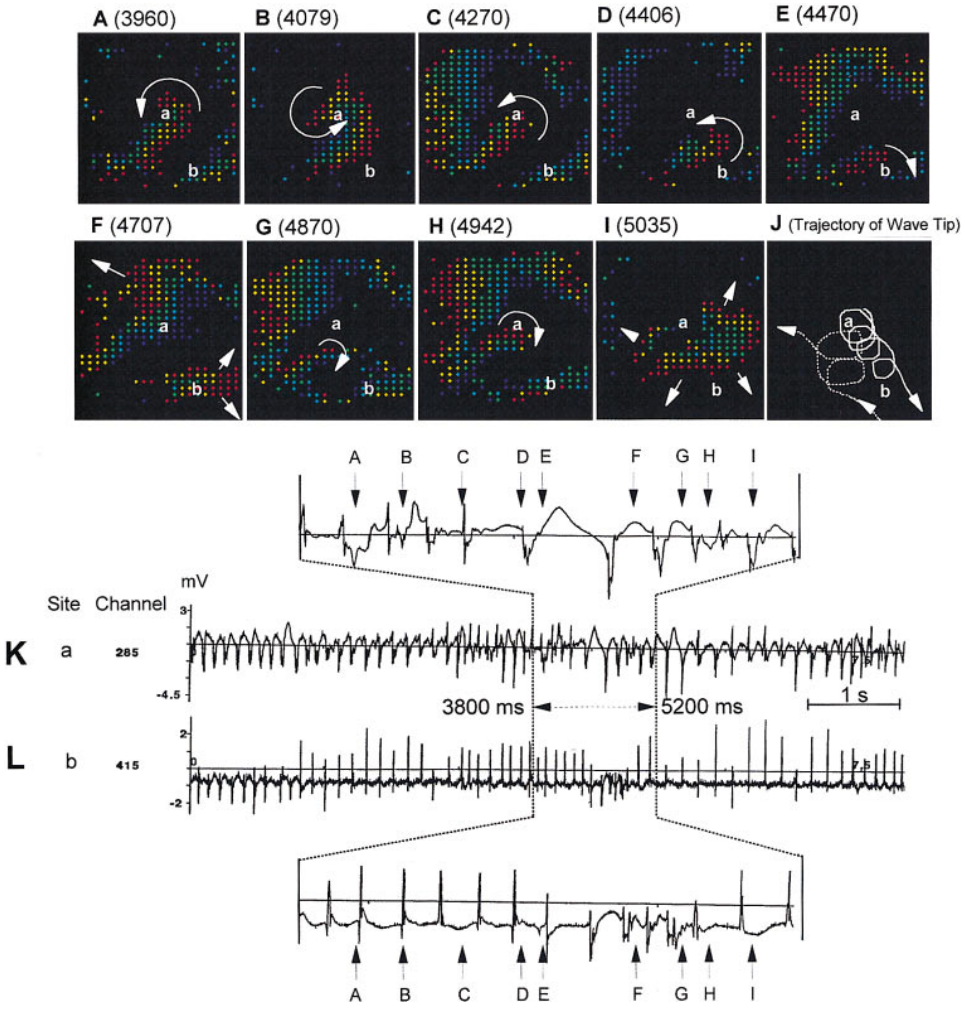

Figure 15. Drifting single reentrant wave front as the source of VF activations. The data were from the pig No. 4. Color panels *A–I* are selected frames from the dynamic display of activation patterns during VF. The time, in milliseconds, of each frame is shown in the parentheses above each frame. (*K* and *L*) Electrogram in or near the core corresponding to sites *a* and *b* in *A–I*. The electrogram recordings were made during the time intervals indicated in *A–I*. In color panels *A–E*, a single reentrant wave front, rotating in a counterclockwise direction, drifted from the center to the right lower quadrant. The electrogram at site *a* was initially inside the core and thus registered double potential (*arrows A* and *B* in panel *K*), whereas electrogram *b* showed single deflection (*arrows A* and *B* in panel *L*). In color panel *E*, the tip of reentrant wave front moved towards the right lower quadrant and the electrogram at site *a* was no longer within the core, while the electrogram at site *b* was inside the core and shows a double deflection (*arrow E* in panel *L*). Thereafter, wave fronts propagated from the lower edge and both sites *a* and *b* were activated (*F*). The tip of a newly formed reentrant wave front rotated in a clockwise direction (color panels *G* and *H*) and visited site *a* (color panel *H*), which registered double potential (*arrow H* in panel *K*). Color panel *I* shows termination of the reentrant wave front by a new wave front arriving from epicardial breakthrough near the core. (*J*) The trajectory of the tip of the reentrant wave front. After the tip trajectory drifted toward right lower quadrant (*solid line*), a new reentrant wave front formed from the lower edge and moved out toward left edge (*dotted line*).

experimental parameter. When considering a claim of a route to chaos, experimentalists prefer to see that route evolve in sequence by experimental manipulation of a single parameter. Here the progressive reduction of tissue mass meets that requirement.

The transition (in reverse) is illustrated by the sequential appearance of the Poincaré plots. Recall that there were three characteristic shapes: cloud-like, ring-like, or point-like. These shapes play significant roles in the quasiperiodic scenario. Cloud-like shapes are consistent with random or high-dimensional chaotic behavior. Ring-like shapes signify quasiperiodicity (4); in these cases, the presence of the heavy concentration of points in a small region on the equilibrium line, (the signet ring) means that the system is frequently near-periodic, with occasional excursions into modulated quasiperiodicity. One advantage of the methods used in this study is that continuous TMP recordings were obtained with high accuracy. This is a significant improvement over previous studies (4) in which only extracellular recordings were available. In extracellular recordings, only the activation times can be considered reliable data, whereas with a TMP recording, the full waveform can be used. Because of this increased resolution, we were able to find the embedding dimension for KE calculation. The entropy progressively decreased when tissue mass was reduced. The fact that the tissue always showed the sequence in the order predicted by the quasiperiodic scenario, and in one animal showed the full sequence with progressive tissue mass reduction, accompanied by the presence of significant low-frequency modulation, supports the relevance of this scenario to cardiac fibrillation.

Critical mass necessary for sustaining VF or VT. The experiment by Garrey (6) was performed without tissue perfusion, which could have caused progressive ischemia and thus affected the ability for VF to sustain itself. In comparison, our tissue was both perfused and superfused, allowing accurate quantitation of the critical mass of VF. Zipes et al. (27) reported that VF was terminated when a critical amount of myocardium became depolarized by either potassium chloride or electrical discharge, and estimated the critical mass for VF as $\sim$ 28% of the total heart weight. In our study, the critical mass for sustaining spontaneous and inducible VF was $\sim$ 16% (24.0 g) and 13% (19.9 g) of total weight of heart, respectively. These

values were less than those of Garrey (25%) (6) or Zipes (28%) (27), but were similar to the 10–20 g value in Langendorff-perfused pig hearts reported by Janse et al. (28). Damiano et al. (29) performed surgical isolation of canine right ventricular free wall during cardiopulmonary bypass. In 9 of 10 dogs studied, VF could not be induced in the isolated right ventricle. However, the weight of isolated right ventricular free wall was not measured. While a critical mass is needed to sustain VF, the absolute value of the critical mass appears to be larger in the canine model than in the swine model. The mechanism by which swine tissue can fibrillate in a smaller mass than the canine tissue is unclear.

Physiological effects of tissue mass reduction on transmembrane potential characteristics. Multiple wavelets with short-lived reentrant wave fronts are characteristics of VF both in the intact ventricles (2) and in the in vitro model of VF used in this study before tissue mass reduction. As the mass of the ventricle was reduced, there was a decrease in the number of wave fronts and therefore the chance for interference (30), resulting in longer life span of organized reentry. Furthermore, because fewer wave fronts were present to compete for the excitable cells, the excitable gap or diastolic interval increased. Because of the restitution properties of cardiac cells, a longer diastolic interval was followed by a longer APD, which in turn increased the size of the core and the period (cycle length) of the rotor (31). Therefore, when the tissue mass was reduced, there was an increase of the cycle length of reentry.

The mechanisms by which the number of wave fronts decreased are unclear. We propose the following explanations. First, cutting results in the elimination of the sources of activations outside the mapped region, which in turn reduced the number of invading wave fronts. Second, wavelets can be terminated by arriving at a boundary of the tissue. An effect of the tissue mass reduction is the increased boundary to mass ratio. When the relative size of boundary is increased, it is more likely for the reentrant wave front and the wavelets to terminate by arriving at a boundary (32, 33). Third, with a decreased number of wavelets, the likelihood that colliding wave fronts will generate new reentrant wave fronts (2) is also further reduced. Other possible mechanisms, such as progressive ischemia and deterioration of the preparations, were ruled out by the results of control studies (protocol-3).

Moe et al. (7) proposed that the generation and maintenance of cardiac fibrillation is determined by the characteristic length (tissue mass), the inverse of conduction velocity, and the inverse of refractory period. The results of this study, however, indicate that these three factors are not independent of each other. Decreasing tissue mass increases APD, hence the refractoriness. While conduction velocity was not measured in this study, the increased $(dV/dt)_{max}$ during tissue mass reduction implies a faster conduction velocity (34). Based on these observations, the mass, the refractory period, and conduction velocity are not independent. Rather, they are closely coupled to each other.

Limitation of the study. Our experiments represent only one of the first steps to understand the complex phenomenon associated with transition from VT to VF in intact ventricles. In addition to tissue mass, the intrinsic electrophysiological heterogeneity (35), the presence of organic heart diseases, and the progressive ischemia induced by prolonged VT could all contribute significantly to the transition of VT to VF and vice versa. These factors were not tested in this experiment. Further experiments are necessary to determine whether or not the quasiperiodic route to chaos hypothesis is applicable to the spontaneous transition from VT to VF in intact human ventricles.

Therapeutic implications. These findings reveal that as tissue mass is decreased, chaos (VF) becomes more low-dimensional before converting to VT. Although tissue mass reduction is not directly feasible as a treatment modality of VF, alterations in tissue geometry that minimize the opportunity for reentrant wave fronts to interact, such as the maze procedure for atrial fibrillation, may act by a similar mechanism. It is also possible that pharmacologic tissue mass reduction by antiarrhythmic drugs, e.g., by increasing the wavelength relative to a fixed tissue mass, may have an equivalent effect. The extent to which the multiple oscillators of a quasiperiodic system are coupled to each other is a strong determinant of whether the behavior exhibited by the system is periodic or irregular. If the factors governing the coupling strength between the oscillators can be identified, they will be promising targets for new antifibrillatory strategies. This study also demonstrates that the spatial complexity of arrhythmias is reflected in the record of the electrical activity at a single site. Monitoring local activity may provide useful information for early detection of the onset of instability leading to VF.

Acknowledgments

We thank Dr. P.K. Shah, Dr. James N. Forrester, and Dr. William J. Mandel for their support, Dustan Hough, Avile McCullen, Meiling Yuan, John Hodgson, and Donald O. Walter for their technical assistance and Elaine Lebowitz for her secretarial assistance. The authors also wish to thank Dr. Peter Hunter, Dr. David Bullivant, Dr. Sylvain Martel, and Serge LaFontaine for constructing the mapping system used in this study.

This study was done during the tenure of a Fellowship Grant from the Department of Medicine, Korea University (Y.-H. Kim), a Cedars-Sinai Burns and Allen Research Institute Fellowship Award (T. Ikeda), a Cedars-Sinai ECHO Foundation Award (H.S. Karagueuzian), an AHA Wyeth-Ayerst Established Investigatorship Award (P.-S. Chen), and was supported in part by National Institutes of Health Specialized Center of Research (SCOR) grant in Sudden Death (P50-HL52319), NIH Research Grants HL50259 and HL44880, and the Ralph M. Parsons Foundation, Los Angeles, CA, and the Kawata and Laubisch Endowments, University of California at Los Angeles.

References

1. Kaplan, D.T. and R.J. Cohen. 1990. Is fibrillation chaos? *Circ. Res*. 67: 886–892.

2. Lee, J.J., K. Kamjoo, D. Hough, C. Hwang, W. Fan, M.C. Fishbein, C. Bonometti, T. Ikeda, H.S. Karagueuzian, and P.-S. Chen. 1996. Reentrant wave fronts in Wiggers' stage II ventricular fibrillation: characteristics, and mechanisms of termination and spontaneous regeneration. *Circ. Res*. 78:660–675.

3. Witkowski, F.X., K.M. Kavanagh, P.A. Penkoske, R. Plonsey, M.L. Spano, W.L. Ditto, and D.T. Kaplan. 1995. Evidence for determinism in ventricular fibrillation. *Phys. Rev. Lett*. 75:1230–1233.

4. Garfinkel, A., P.-S. Chen, D.O. Walter, H.S. Karagueuzian, B. Kogan, S.J. Evans, M. Karpoukhin, C. Hwang, T. Uchida, M. Gotoh, et al. 1997. Quasiperiodicity and chaos in cardiac fibrillation. *J. Clin. Invest*. 99:305–314.

5. Ruelle, D., and F. Takens. 1971. On the nature of turbulence. *Comm. Math. Phys*. 20:167–192.

6. Garrey, W.E. 1914. The nature of fibrillatory contraction of the heart—its relation to tissue mass and form. *Am. J. Physiol*. 33:397–414.

7. Moe, G.K., W.L. Rheinboldt, and J.A. Abildskov. 1964. A computer model of atrial fibrillation. *Am. Heart J*. 64:200–220.

8. Nearing, B.D., A.H. Huang, and R.L. Verrier. 1991. Dynamic tracking of cardiac vulnerability by complex demodulation of the T wave. *Science*. 252: 437–440.

9. Ikeda, T., T. Uchida, D. Hough, J.J. Lee, M.C. Fishbein, W.J. Mandel, P.-S. Chen, and H.S. Karagueuzian. 1996. Mechanism of spontaneous termination of functional reentry in isolated canine right atrium: evidence for the presence of an excitable but nonexcited core. *Circulation*. 94:1962–1973.

10. Bonometti, C., C. Hwang, D. Hough, J.J. Lee, M.C. Fishbein, H.S. Karagueuzian, and P.-S. Chen. 1995. Interaction between strong electrical stimulation and reentrant wavefronts in canine ventricular fibrillation. *Circ. Res*. 77: 407–416.

11. Kobayashi, Y., W. Peters, S.S. Khan, W.J. Mandel, and H.S. Karagueuzian. 1992. Cellular mechanisms of differential action potential duration restitution in canine ventricular muscle cells during single versus double premature stimuli. *Circulation.* 86:955–967.

12. Chen, P.-S., P. Wolf, E.G. Dixon, N.D. Danieley, D.W. Frazier, W.M. Smith, and R.E. Ideker. 1988. Mechanism of ventricular vulnerability to single premature stimuli in open chest dogs. *Circ. Res*. 62:1191–1209.

13. Chen, P.-S., P. Wolf, F.J. Claydon, E.G. Dixon, H. Vidaillet, Jr., N.D. Danieley, T.C. Pilkington, and R.E. Ideker. 1986. The potential gradient field created by epicardial defibrillation electrodes in dogs. *Circulation.* 74:626–636.

14. Gilmour, R.F., M. Watanabe, and D.R. Chialvo. 1993. Low dimensional dynamics in cardiac tissues. Experiments and theory. *In* Chaos in Biology and Medicine. W.L. Ditto, editor. SPIE-The International Society for Optical Engineering, Bellingham, WA. 2–9.

15. Kolmogorov, A.N. 1958. A new metric invariant of transitive dynamical systems and automorphisms in Lebesgue spaces. *Dokl. Akad. Nauk SSSR.* 119: 861–864.

16. Sinai, Y.G. 1959. On the concept of entropy of a dynamical system. *Dokl. Akad. Nauk SSSR.* 124:768–778.

17. Hilborn, R.C. 1994. Chaos and nonlinear dynamics. Oxford University Press, New York. 386–390.

18. Kennel, M.B., R. Brown, and H.D.I. Abarbanel. 1992. Determining embedding dimension for phase-space reconstruction using a geometrical construction. *Phys. Rev.* 45:3403–3411.

19. Friedman, P. 1995. GB-Stat. Dynamic Microsystems, Inc., Silver Spring, Maryland.

20. Gray, R.A., J. Jalife, A. Panfilov, W.T. Baxter, C. Cabo, J.M. Davidenko, and A.M. Pertsov. 1995. Nonstationary vortexlike reentrant activity as mechanism of polymorphic ventricular tachycardia in the isolated rabbit heart. *Circulation.* 91:2454–2469.

21. Starmer, C.F., D.N. Romashko, R.S. Reddy, Y.I. Zilberter, J. Starobin, A.O. Grant, and V.I. Krinsky. 1995. Proarrhythmic response to potassium channel blockade. Numerical studies of polymorphic tachyarrhythmias. *Circulation*. 92:595–605.

22. Grassberger, P. 1989. Information content and predictability of lumped and distributed dynamical systems. *Physica Scripta.* 40:346–353.

23. Chate, H. 1995. On the analysis of spatiotemporally chaotic data. *Physica D*. 86:238–247.

24. Cross, M., and P. Hohenberg. 1993. Pattern formation outside of equilibrium. *Rev. Mod. Phys*. 65:851–1112.

25. Deleted in Proof.

26. Brandstater, A., and H. Swinney. 1987. Strange attractors in weakly turbulent Couette-Taylor flow. *Phys. Rev.* 35:2207–2220.

27. Zipes, D.P., J. Fischer, R.M. King, A.D. Nicoll, and W.W. Jolly. 1975. Termination of ventricular fibrillation in dogs by depolarizing a critical amount of myocardium. *Am. J. Cardiol.* 36:37–44.

28. Janse, M.J., F. Wilms-Schopman, and R. Coronel. 1995. Ventricular fibrillation is not always due to multiple wavelet reentry. *J. Cardiovasc. Electrophysiol*. 6:512–521.

29. Damiano, R.J., Jr., T. Asano, P.K. Smith, T.B. Ferguson, Jr., J.M. Douglas, Jr., and J.L. Cox. 1986. Electrophysiologic effects of surgical isolation of the right ventricle. *Ann. Thorac. Surg*. 42:65–69.

30. Cha, Y.-M., U. Birgersdotter-Green, P.L. Wolf, B.B. Peters, and P.-S. Chen. 1994. The mechanisms of termination of reentrant activity in ventricular fibrillation. *Circ. Res*. 74:495–506.

31. Zykov, V.S. 1987. Simulation of the process of circulation of an excitation in heart muscle. *In* Simulation of Wave Processes in Excitable Media. A.T. Winfree, editor. Manchester University Press, Manchester. 93–112.

32. Ong, J.J.C., J.J. Lee, L.S. Tseng-Ong, H.S. Karagueuzian, and P.-S. Chen. 1996. Anatomic boundaries as a mechanism for termination of meandering reentrant wave fronts during atrial fibrillation. *Circulation*. 94:I-351(Abstr.).

33. Yermakova, Y.A., and A.M. Pertsov. 1986. Interaction of rotating spiral waves with a boundary. *Biophysics (Eng. Trans. Biofizika)*. 31:932–940.

34. Levine, J.H., E.N. Moore, H.F. Weisman, A.H. Kadish, L.C. Becker, and J.F. Spear. 1987. Depression of action potential characteristics and a decreased space constant are present in postischemic, reperfused myocardium. *J. Clin. Invest*. 79:107–116.

35. Antzelevitch, C., S. Sicouri, S.H. Litovsky, A. Lukas, S.C. Krishnan, J.M. Di Diego, G.A. Gintant, and D. Liu. 1991. Heterogeneity within the ventricular wall. Electrophysiology and pharmacology of epicardial, endocardial, and M cells. *Circ. Res*. 69:1427–1449.